# Deposition characteristics of copper particles on roughened substrates through kinetic spraying

S. Kumar, Gyuyeol Bae, Changhee Lee [*]

*Kinetic Spray Coating Laboratory (National Research Laboratory), Division of Materials Science and Engineering, Hanyang University, Seoul, Republic of Korea*

## ARTICLE INFO

## ABSTRACT

In this paper, a systematic study of copper particle deposition behavior on polished and roughened surfaces (aluminum and copper) in kinetic spray process has been performed. The particle deformation behavior was simulated through finite element analysis (FEA) software ABAQUS explicit 6.7–2. The particle–substrate contact time, contact temperature and contact area upon impact have been estimated for smooth and three different roughened substrate cases. Copper powders were deposited on smooth and grit-blasted copper and aluminium substrates and characterized through scanning electron microscopy and Romulus bond strength analyzer. The results indicate that the deformation and the resultant bonding were higher for the roughened substrates than that of smooth. The characteristic factors for bonding are reported and discussed. Thus the substrate roughness appears to be beneficial for the initial deposition efficiency of the kinetic spray process.

## 1. Introduction

In conventional atmospheric spray technologies, spray materials are exposed to higher temperature and an oxidizing environment during flight, which leads to oxidation and phase transformation. Over a decade of development, kinetic spraying has been successful in depositing a wide range of pure metals, metal alloys, polymers, composites and nano-materials onto a variety of substrate materials [1–4]. Kinetic spray deposition occurs when small solid-state particles are accelerated to supersonic velocity, and then impacted onto a substrate. The gas and particle temperatures remain below melting temperature of sprayed materials. The deposition process between in-flight feedstock particle and substrate finishes within a very short time period. The adhesion mechanism in the kinetic spray process completely differs from that of conventional thermal spraying. It is based on severe plastic deformation or shear instability between solid plastic flow of particle and substrate materials [5–7]. The plastic deformation depends more on the material properties of feedstock and substrate more than on the impact particle velocity.

The interface reactions due to high velocity impact have not been well understood, even though many different interfacial reactions have been documented by experimental and theoretical investigations. Sufficient kinetic energy must be available for plastic deformation of the materials. The kinetic energy of the particles plays a central role in the impact and deformation behaviors. Kinetic spraying can cause high contact stress, particle strain and strain rate. Metallic bonding is observed in the coatings; hence, surface adhesion is believed to play an important role in the particle bonding. Nano/micro-scale material mixing and mechanical interlocking were identified and used to explain the enhancement of interfacial bonding [8]. Mechanical anchorage, physical adhesion and metallic interactions are involved in all kinds of interfacial reactions. Thus, it is believed that the rougher coating surface causes higher mechanical anchorage. High contact pressures are believed to be necessary conditions for particle/substrate and particle/pre-deposited material bonding. The contact pressure at the interface is proportional to contact area and kinetic energy of particle. The impact of single particle of various materials on flat substrate surfaces for different velocities was modeled by using the finite element program ABAQUS [6,9]. Many authors indicated that particle conditions prior to impact, such as particle velocity, temperature, size and particle impacting angles will influence the deformation behaviors of particles. The effect of

* Corresponding author. Tel.: +82 2 2220 0388; fax: +82 2 2293 4548.
  *E-mail address:* chlee@hanyang.ac.kr (C. Lee).

substrate roughness on the different coating properties has been analyzed by many authors in thermal plasma spraying [10–14]. Substrate roughness effect in kinetic spraying was researched by very few authors [3,15,16] experimentally. In this study, the effect of substrate roughness on the deposition and deformation of particle has been studied through modeling and compared with the experimental results.

## 2. Experiment

### 2.1. Experimental approach

A commercially available CGT kinetic spraying system was used for deposition. The equipment and the coating process are described elsewhere in the literature [17,18]. Nitrogen was used as process and carrier gas. The process parameters and corresponding velocity of the 25 μm copper powder was estimated by empirical equation [17] and listed in Table 1.

Process gas pressure and temperature were used for controlling the impact velocity. Copper and aluminium plates were used as substrates. Prior to deposition, the substrates were cut to the desired dimensions and subjected to different surface preparations. For smooth substrates, the plates were polished as smooth as a metal mirror. Roughened substrates were prepared through grit blasting. The average grain size of alumina grits is 46 meshes and the grit blasting was carried out for 1 min. The gun axis was fixed perpendicular to the surface of the substrate. The substrates were subsequently cleaned by supersonic washing. The substrate distance from the exit of the nozzle was fixed at 30 mm. The feedstock powders were deposited through kinetic spraying by using nitrogen as a powder carrier gas with low (4 g/min) and high (20 g/min) feed rate for getting individual deposition and full coating, respectively.

The top view and cross-sectional observations of both the individual and full coatings were performed through scanning electron microscopy (SEM). Deposition efficiency, which is the weight fraction of deposited coatings divided by the total powder utilized, is normally used to evaluate the coating efficiency in thermal and kinetic spraying. The bond strength was carried out using a non-standard Romulus Bond Strength Tester. The coating specimens were cut to 8 mm × 12 mm rectangles. Aluminium test studs were attached to the micro-polished coating surfaces. A unique ultra strong (85 MPa) epoxy bonding agent was applied to the test stud assemblies and thermally cured at 200 °C for 90 min. The bond strengths were evolved.

### 2.2. Numerical simulation

The deformation behavior of the copper particle on smooth and roughened surfaces was modeled using ABAQUS 6.7–2 finite element analysis software, which accounted for strain hardening, strain-rate hardening, thermal softening and heating due to frictional, plastic and viscous dissipation. Axisymetric analysis was performed, in which adaptive meshing was used to overcome large deformations near the contact areas. Analysis was done for 25 μm spherical copper powder. Arbitrary Lagrangian Eulerian

(ALE) method is commonly used to avoid the problems (mathematical truncation error) associated with the severe deformation of meshing. A smooth and three different kinds of roughened substrates were assumed for modeling, which are: (a) the roughness of the substrate is half the particle size (crest-1 and trough-1), (b) same as particle size and (crest-2 and trough-2) and (c) twice the particle size (crest-3 and trough-3). The impacts of powder were considered on crest and trough parts of each substrate roughness. Fig. 1 shows the axisymetric models and initial meshing conditions of the impact models.

In order to simulate and analyze the deformability of the powder and the substrate under different impact conditions, the use of strain rate-dependent and temperature-dependent constitutive description is required in finite element codes. Typically, the stress is expressed as a function of strain, strain rate, and temperature. A number of physically based constitutive models have been proposed. Due to its simple multiplication form, the empirically based Johnson–Cook (J–C) model was used to describe the plastic flow of material to explain the mechanical behavior of metals at high strain rates and various temperatures. The material deformation behavior of both particle and substrate was described by the Johnson–Cook plasticity model, which accounts for strain hardening, strain-rate hardening and thermal softening effects. The equivalent flow stress is explained as:

$$\sigma = \left[A + B\varepsilon_{\mathrm{p}}^{n}\right]\left[1 + C\ln\left(\frac{\dot{\varepsilon}_{\mathrm{p}}}{\dot{\varepsilon}_{0}}\right)\right]\left[1 - (\mathrm{T}^{*})^{m}\right] \qquad (1)$$

where $A$, $B$, $n$, $C$ and $m$ are the material dependent constants. $\dot{\varepsilon}_{\mathrm{p}}$ is the effective plastic strain rate and $\dot{\varepsilon}_{0}$ is the normalized reference strain rate. The model parameters can be obtained by compression quasi-static and dynamic Hopkinson bar experiments with varying temperature and strain rates. $T^{*}$ is normalized temperature. For modeling, copper was taken as a reference particle material, whereas copper and aluminium were used as reference substrate materials. The material parameters are shown in Table 2 which were taken from the literature [19,20]. The temperature rise is based on the empirical assumption that 90% of plastic work under adiabatic conditions is dissipated as heat. Impact velocity of the copper powder was increased from 300 to 600 m/s The substrate and particle temperature prior to impact is considered to be at room temperature.

## 3. Results and discussion

### 3.1. Feedstock characterization

Fig. 2a and b shows the morphology and size distribution of gas atomized copper feedstock powders characterized through scanning electron microscopy and laser scattering technique,

**Table 1**
Process parameters and corresponding impact velocity.

| Process gas temperature (°C) | Process gas pressure (bar) | Corresponding impact velocity (m/s) |
|---|---|---|
| 400 | 20 | 530 |
| 450 | 25 | 570 |
| 500 | 30 | 600 |

**Table 2**
Simulation parameters for copper and aluminium.

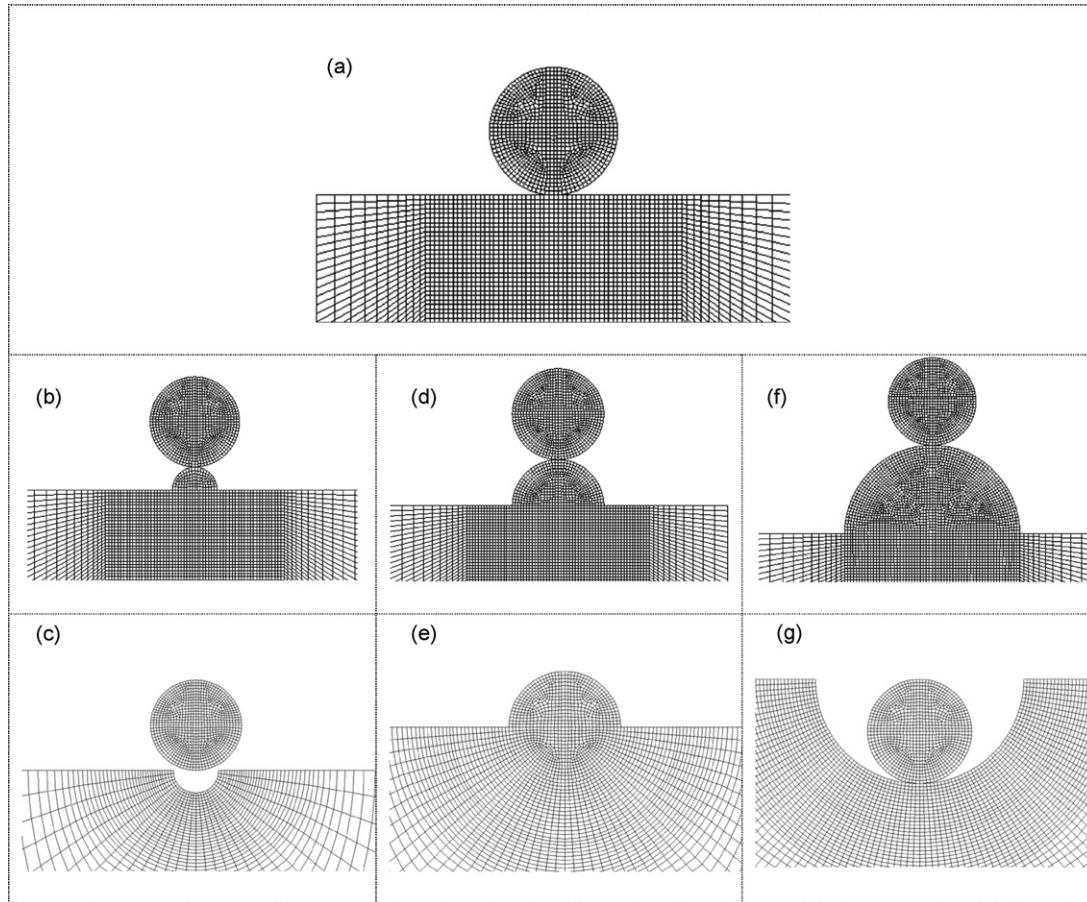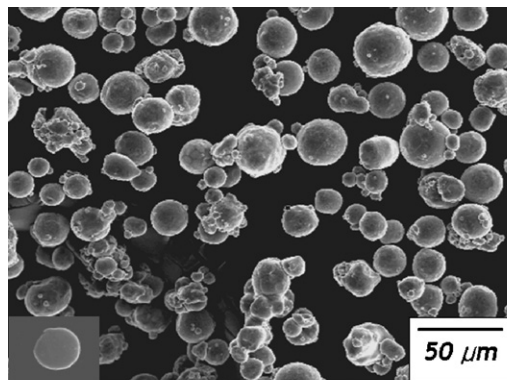| Parameter/material | Aluminum (Al) | Copper (Cu) |
|---|---|---|
| Density (kg/m$^3$) | 2710 | 8960 |
| Young's modulus (GPa) | 68.9 | 124 |
| Poison's ratio | 0.33 | 0.34 |
| Heat capacity (J/kg K) | 904 | 383 |
| Melting temperature (K) | 916 | 1356 |
| $A$ (MPa) | 148.4 | 90 |
| $B$ (MPa) | 345.5 | 292 |
| $n$ | 0.183 | 0.31 |
| $C$ | 0.001 | 0.025 |
| $m$ | 0.895 | 1.09 |
| Reference temperature (K) | 293 | 298 |
| Reference strain rate (1/s) | 1 | 1 |

Fig. 1. Initial mesh configuration of the impact models for 25 μm powder.

respectively. It is seen from the figure that the shape of the powders is spherical without any sharp corners. The inner figure shows the cross-section of the copper powder. The mean size of the feedstock powder was estimated to be 24.62 μm.
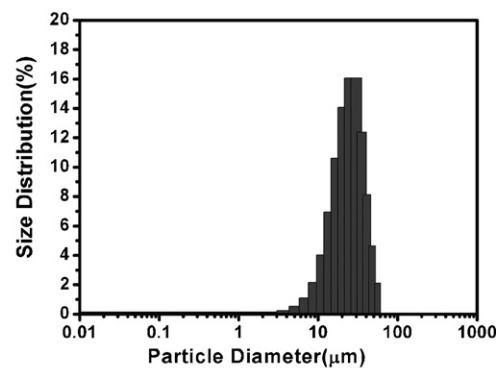
### 3.2. Individual deposition characterization

Individual particles impacted onto the substrates, and cross-section of single particle deposition could be obtained through scanning electron microscopy. The deposition surfaces and bonded particles for different substrate surfaces were observed. Fig. 3a (smooth), b (impacted on roughness with half the particle size – crest part), c (impacted on roughness with same as particle size – crest part) and d (impacted on roughness with twice as particle size – crest part) shows simulated shapes of the deposited copper particles on different aluminum substrates having different roughness values for 570 m/s impact velocity. Fig. 3e shows the cross-section of embedded copper particles onto smooth aluminum substrate and Fig. 3f–h show the same for grit-blasted substrates. The corresponding velocity was estimated as 570 m/s through empirical formula. As the grit blasting was performed using different shape and size powders, the grit-blasted substrates have different roughness shapes. It is clear from Fig. 3, that the deformation of the particles at same velocity on different



(a) Morphology and cross section of powder

(b) Particle size distribution

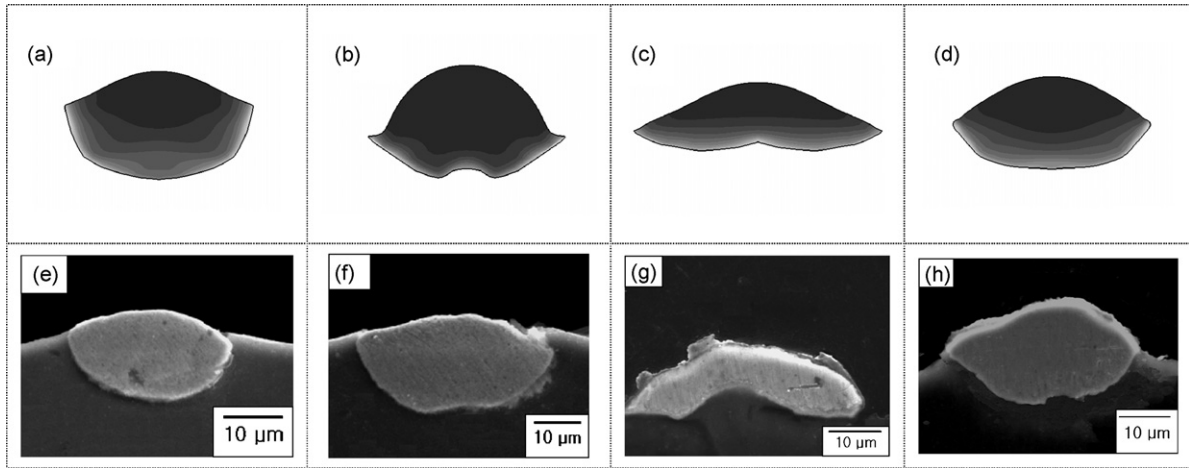Fig. 2. SEM image and size distribution of feedstock powder.

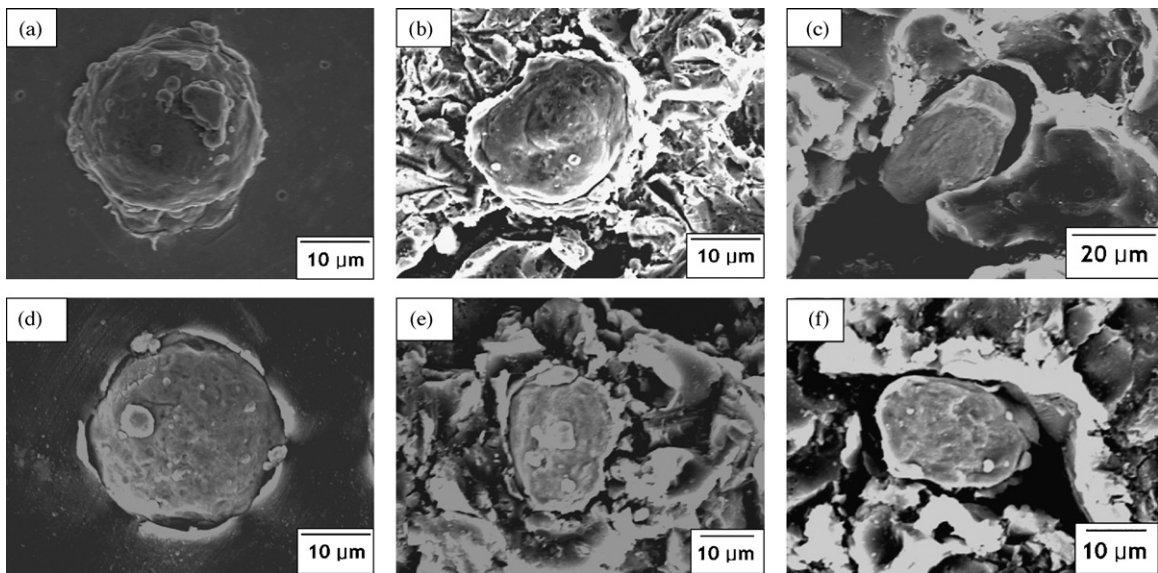**Fig. 3.** Cross-section of deposited powders on different substrates and corresponding simulated images.



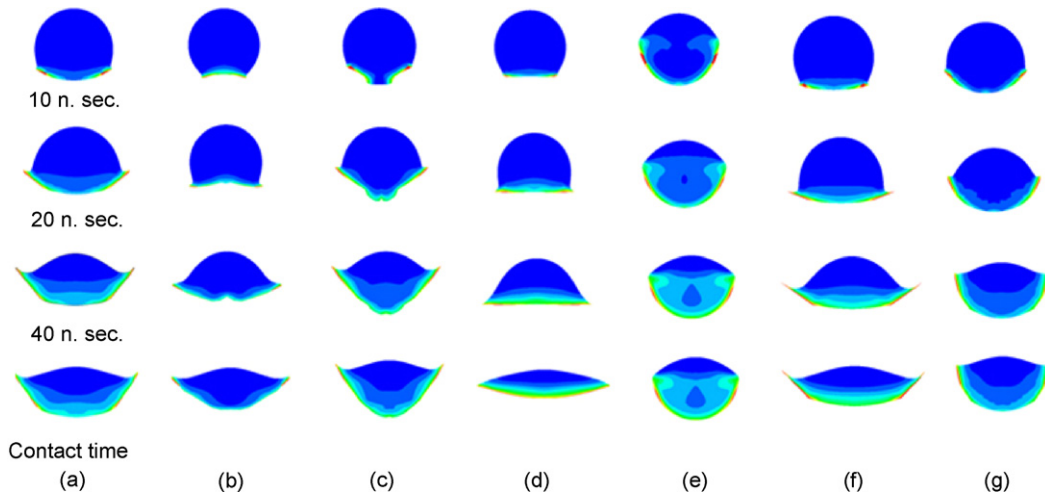**Fig. 4.** Individual particle deposition on substrates and mechanical interlocking.



**Fig. 5.** Impact behavior of particles on different substrates. (a) Planar; (b) crest size half of particle size; (c) trough size half of particle size; (d) crest size same as particle size; (e) trough size same as particle size; (f) crest size twice of particle size; (g) trough size twice of particle size.

substrates has different characteristics. The flattening ratios of particles impacted onto smooth surface and rough surfaces with crest values of, respectively, 12.5, 25 and 50 μm were 1.53, 1.66, 2.02, and 1.89, respectively. Increasing roughness increases the flattening or deformation of the particles up to a certain value of crest size. It is noted that the flattening ratio, defined as the ratio of the diameter of the bonded particle to that of a spherical particle of the same volume, is used for estimating the deformation of

impacted particle. The maximum deformations of the particles have been achieved for the substrate roughness similar to the particle size which can be seen from Fig. 3c and g. Further increase in the roughness value decreases the deformation or flattening of the deposited powders. For higher roughness values, the deposition characteristics are similar as the smooth substrates according to the cross-section images of the particles and the simulated shapes of the deposited particles. In the rough surface, the crest
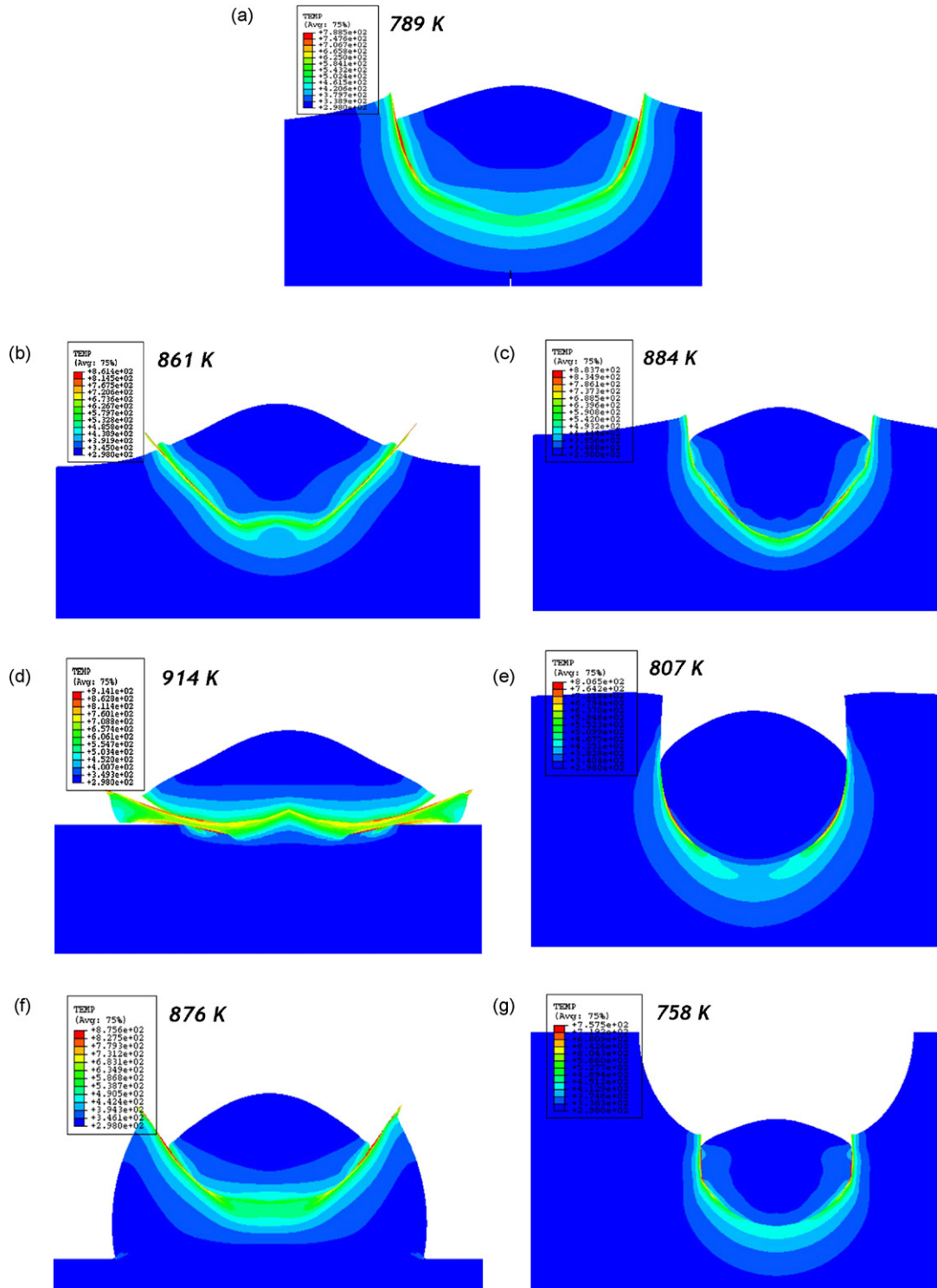


**Fig. 6.** Interface temperature at contact time for different cases. (a) Planar; (b) half the particle size crest; (c) half the particle size trough; (d) same as particle size crest; (e) same as particle size trough; (f) twice the particle size crest; (g) twice the particle size trough.
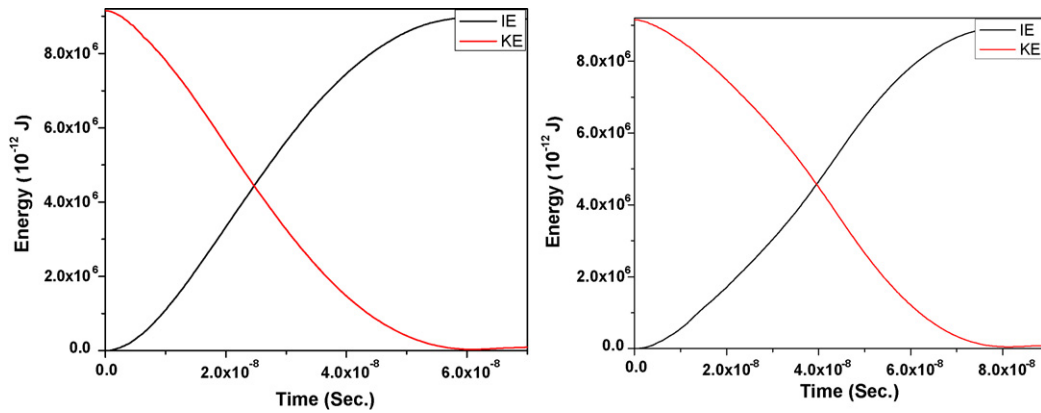
**Fig. 7.** Energy diagram of impact for planar and roughened substrates. IE, internal energy and KE, kinetic energy.

with maximum surface area and low curvature has the characteristic nature similar to that of smooth substrate during impact. In order to get the clear picture about the effect of roughness, scanning electron microscope images of the top view of the individually deposited powders on different substrates are shown in Fig. 4a–f. From the top view, it is clear that the deposition behaviors are similar for all the cases. Fig. 4c and f shows the mechanically interlocked copper particles on grit-blasted copper and aluminum substrates, respectively.

### 3.3. Numerical simulation results

In order to get a clear idea about the interface parameters such as contact time, contact temperature and contact area, numerical modeling results have been discussed. Fig. 5a (smooth), b (crest similar as half the particle size), c (trough similar as half the particle size), d (crest similar as particle size), e (trough similar as particle size), f (crest similar as twice the particle size) and g (trough similar as twice the particle size) shows the deformation patterns of 25 μm copper particles impacting on smooth copper and roughened copper substrates, respectively, at constant velocity. It is obvious from the figures that at a given time interval, the deformation is more for the particles impact on the roughened substrates except on trough whose size is similar to the particle size. The flattening characteristics for different substrates are different as discussed earlier.

Fig. 6 shows the deformed pattern of the copper particles on different aluminum substrates at same impact velocity and the corresponding interface temperature values. From the simulation data, it is clear that increasing impact velocity increases the interface temperature. In Fig. 6, the interface temperature for roughened substrates (for crest size of half the particle size: 861 K; for trough size of half the particle size: 884 K; for crest size same as particle size: 914 K; for trough size same as particle size: 807 K; for crest size twice the particle size: 876 K) at contact time are higher than that of smooth case (789 K). And among roughened substrates, the interface temperature for crest size which is same as particle size is higher among all the cases. The strain values are in the same tendency. Among the crest cases, the crest whose size is same as the particle size has higher interface temperature. But in the case of trough, the trough whose size is just half the particle size has higher interface temperature.

From the interfaces of the deformed particles, it is clear that the maximum interface temperature distributions for smooth and highly roughened substrate are localized in a small region. However, in roughness cases, where roughness value is similar to that of particle size, the maximum temperature distribution is along the interface between particle and substrate contact region.

Fig. 7 shows energy diagram of the impacted particles on smooth and on crest whose size is same as particle size which indicates that the contact time of the particle with substrate for the roughened substrate is higher than that of smooth substrate.

The high plastic strain-induced softening can dominate against hardening effects at higher velocities and lead to an adiabatic shear instability at the interface. This adiabatic shear instability at the interface could play a significant role in the bonding mechanism.

The bonding mechanism can be influenced by factors such as contact surface area, contact time and contact temperature, etc. Fig. 8 shows the contact times for different cases. It is clear from the figure that the contact times for roughened surfaces are relatively higher than that of smooth. From the modeling data, the contact time increases with increasing impact velocity of the particles for smooth case. The data clearly shows that the similarity between smooth and roughness having high crest area.

Fig. 9 shows the comparison of contact area of particle impacts on smooth and crest part of roughened substrates for different impact velocities. It is clear that increasing impact velocity increases the contact area values. Fig. 10 shows the contact time and contact area for the particle impact on a smooth, three different crest and trough locations of the substrates. In general, both the contact time and contact area are higher for crest regions and lower for trough region. However, trough size which is half the particle size shows higher contact area and contact time than smooth case. Wu et al. [17] explained that the adhesion energy is a
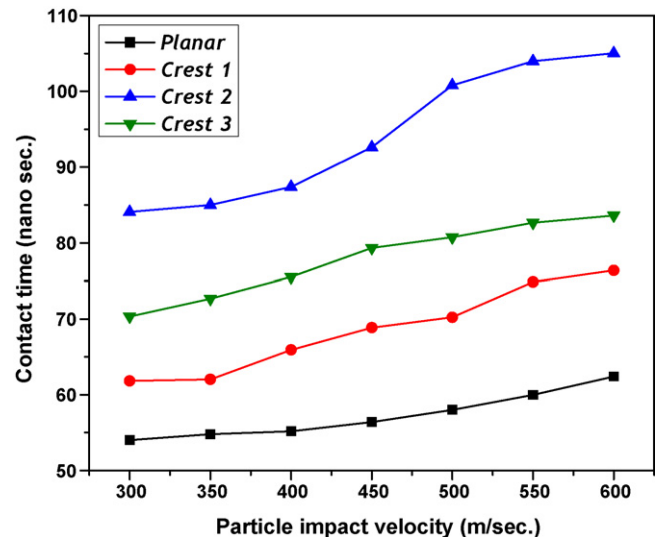


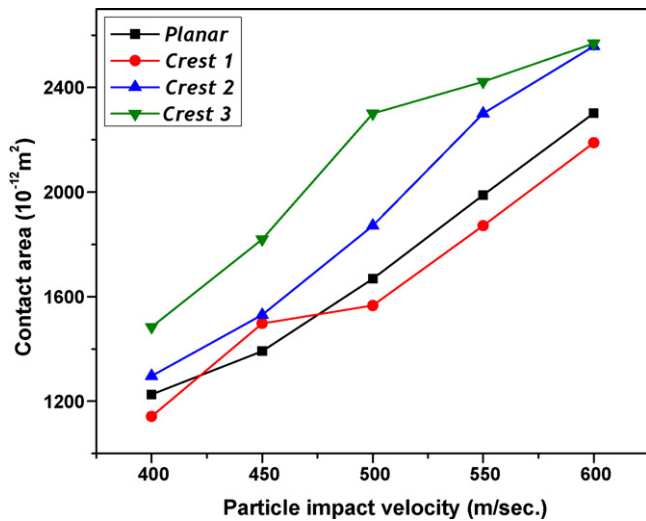**Fig. 8.** Contact time as a function of particle velocity.

Fig. 9. Contact area as a function of particle impact velocity.



Fig. 10. Contact area and contact time for different cases.

function of contact area, contact temperature and contact time. Assadi et al. [6] explained that the formation of the jet for the second particle is influenced by the change in morphology and properties of the underlying substrate as a result of the first impact.

### 3.4. Coating characterization

Fig. 11a–d shows the cross-sectional microstructure of the coatings prepared on smooth copper, smooth aluminium, grit-blasted copper and grit-blasted aluminium substrates, respectively. The process parameters were same as those used for individual deposition for all the coatings. In order to clearly reveal the interface between the deposit and the substrate, chemical etching was carried out for copper substrate case. The etchant
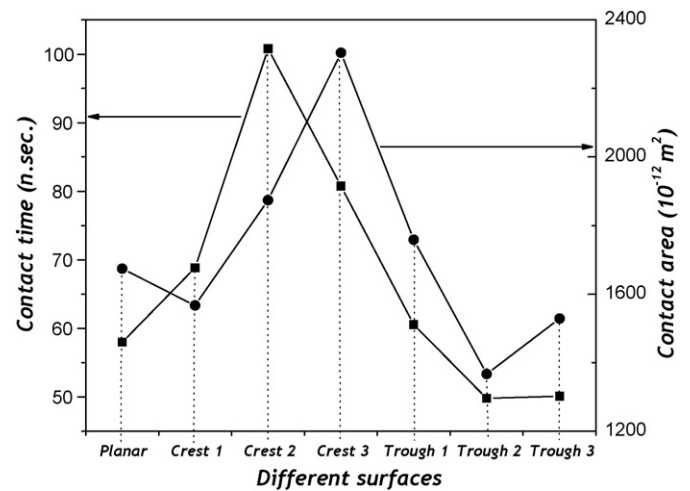
contained 30 ml hydrochloric acid and 10 g of iron(III) chloride dissolved in 120 ml distilled water. The samples were dipped into the etching solution for 30 s. For successful bonding, the localized plastic deformation of impacted particle is required. From the figures it is clear that the cracks and porosity are quantitatively same for coatings prepared on smooth and grit-blasted substrates. The distribution of defects is also identical. This suggests that the coatings prepared on different substrates have similar properties except for a few layers which are deposited initially. The deposition efficiency was measured and the values were found to be little higher for grit-blasted substrates. The deposition efficiencies for smooth and grit-blasted surfaces were estimated to be 62.7 and 65.2%, respectively. This could be possible due to the influence of roughness and its effect on deformation process and can be
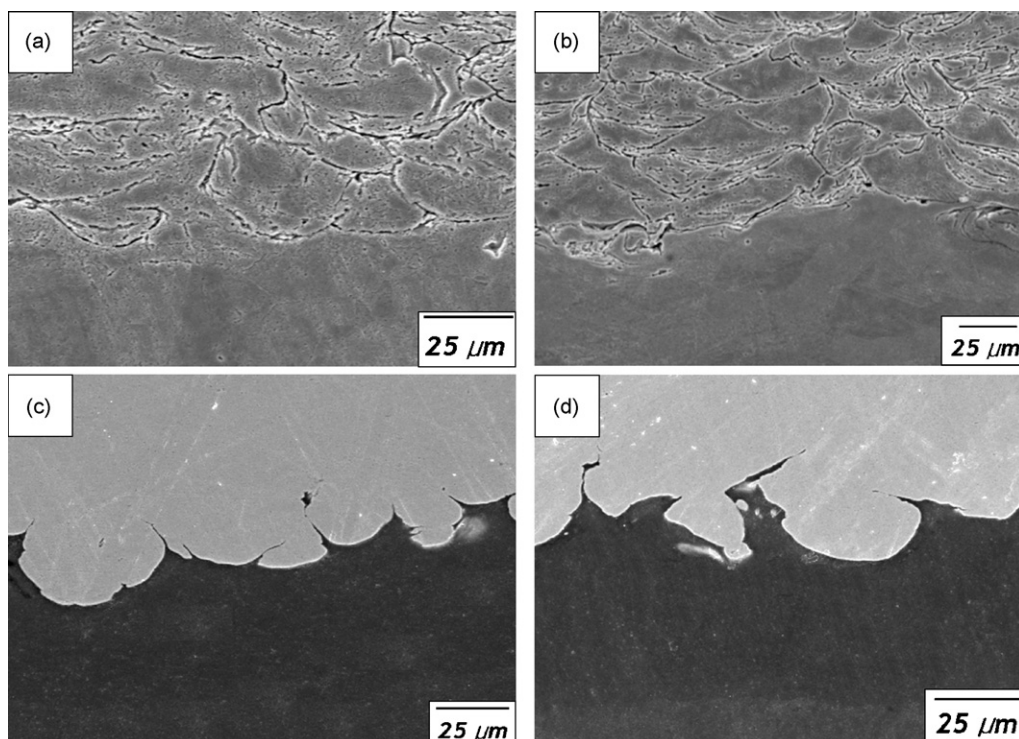


Fig. 11. Cross-section of coatings. (a) Planar copper, (b) grit-blasted copper, (c) planar aluminium and (d) grit-blasted aluminium.
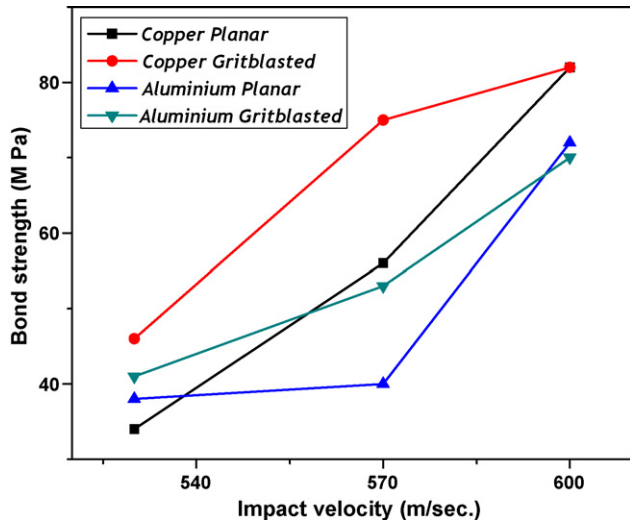
**Fig. 12.** Bond strength results as a function of impact velocity.

supported from Fig. 4c and f. It is also observed that almost all the particles were deposited on grit-blasted substrates, whereas, in the case of smooth substrates many craters could be obtained for the same process conditions.

In order to characterize the initial layers of the coatings, bond strength measurement was carried out. Adhesion strength is considered as the most important mechanical property. Fig. 12 shows the measured bond strength value for different coatings at different process conditions. The coating layers used for stud pull test have more than 250 μm thickness. During the test, the coatings were removed along with studs, thus leaving small fragments on the fracture surface.

From Fig. 12, it is seen that the bond strength for grit-blasted substrates are higher than that of the smooth substrate. It is observed that the relatively higher bond strength has been achieved through kinetic spray process for both the smooth and grit-blasted substrate cases. It is also suggested that either a higher fraction of bonded existing atoms between the surfaces or predominant mechanical interlocking can be responsible for relatively higher bonding strength. Mechanical anchorage is involved in bonding mechanism. It can be a dominant mechanism in high-speed interaction [3,8]. The initial bonding is defined by adiabatic shear instability and mechanical interlocking.

## 4. Conclusion

A systematic approach of copper particle deformation on smooth and roughened copper and aluminium substrates has been performed numerically and experimentally. The following conclusions have been made from the findings.

Impacting particles get deformed more severely on roughened substrate than the smooth cases to obtain higher temperature and strain values. The contact time, contact area and interface temperature are higher on the crest part of roughened substrates, and start decreasing when increasing crest roughness values further. It is suggested that substrate roughness whose crest size is same as particle size and the trough size is half the particle size is beneficial. Bond strength values for grit-blasted substrates are higher than the smooth cases due to the enhanced mechanical interlocking which plays an important role in bonding mechanism.

Hence, it is concluded that grit blasting or roughening of substrate will be useful for successful bonding and further coating formation in kinetic spray process. It could be helpful for the tedious deposition cases in kinetic spray process such as soft particle on hard substrate and vice versa. Further research to optimize the roughness value is essential for different cases.

## Acknowledgement

## References

[1] W. Kroemmer, P. Heinrich, P. Richter, Int. Therm. Spray, Orlando, May 5–8, ASM Int., Materials Park, OH, USA, 2003, pp. 97–102
[2] R.E. Blose, T.J. Roemer, A.J. Mayer, D.E. Beatty, A.N. Papyrin, Int. Therm. Spray, Orlando, May 5–8, ASM Int., Materials Park, OH, USA, 2003, pp. 103–110
[3] J. Wu, J. Yang, H. Fang, S. Yoon, C. Lee, Appl. Surf. Sci. 252 (2006) 7809–7814.
[4] J. Karthikeyan, C.M. Kay, Int. Therm. Spray, Orlando, May 5–8, ASM Int., Materials Park, OH, USA, 2003, pp. 117–121
[5] M. Fukumoto, et al., Thermal Spray, Global Coating Solutions, Ohio, USA, 2007, pp. 96–101.
[6] H. Assadi, F. Gartner, T. Stoltenhoff, H. Kreye, Acta Mater. 51 (2003) 4379–4394.
[7] W. Li, H. Lino, C. Li, G. Li, C. Coddet, X. Wang, Appl. Surf. Sci. 253 (2006) 2852–2862.
[8] M. Grujicic, J.R. Saylor, D.E. Beasley, W.S. DeRosset, D. Helfritch, Appl. Surf. Sci. 219 (2003) 211–227.
[9] F. Gartner, T. Schmidt, T. Stoltenhoff, H. Kreye, Adv. Eng. Mater. 8 (7) (2006) 611–618.
[10] E. Celik, A.S. Demirkiran, E. Avci, Surf. Coat. Technol. 116–119 (1999) 1061–1064.
[11] Y.Y. Wang, C.J. Li, A. Ohmori, Thin Solid Films 485 (2005) 141–147.
[12] R.S.C. Pardes, S.C. Amico, A.S.C.M. d'Oliveira, Surf. Coat. Technol. 200 (2006) 3049–3055.
[13] G. Reisel, R.B. Heimann, Surf. Coat. Technol. 185 (2004) 215–221.
[14] H. Liu, E.J. Lavernia, R.H. Rangel, Acta Metall. Mater. 43 (5) (1995) 2053–2072.
[15] P. Richer, B. Jodoin, L. Ajdelsztajn, E.J. Lavernia, J. Therm. Spray Technol. 15 (2) (2006) 246–254.
[16] H. Yang, H. GWang, X.P. Cao, L. Wang, in: Proceedings of the 2006 International Thermal Spray Conference, May 15–18, Seattle, Washington, USA, 2006.
[17] J. Wu, H. Fang, S. Yoon, H. Kim, C. Lee, Scr. Mater. 54 (2006) 665–669.
[18] S. Yoon, H. Kim, C. Lee, Surf. Coat. Technol. 201 (24) (2007) 9524–9532.
[19] M. Fukumoto, H. Wada, K. Tanabe, M. Yamada, E. Yamaguchi, A. Niwa, M. Sugimoto, M. Izawa, J. Therm. Spray Technol. 16 (2007) 643–650.
[20] N.K. Gupta, M.A. Iqbal, G.S. Sekhon, Int. J. Impact Eng. 32 (2006) 1921–1944.